Supplement of Atmos. Chem. Phys., 22, 15887–15907, 2022
https://doi.org/10.5194/acp-22-15887-2022-supplement


Atmospheric Chemistry and Physics
Open Access
EGU

*Supplement of*

# A global climatology of ice-nucleating particles under cirrus conditions derived from model simulations with MADE3 in EMAC

**Christof G. Beer et al.**

*Correspondence to:* Christof Beer (christof.beer@dlr.de)

This Supplement contains additional information concerning the calculation of ammonium sulfate phase transitions in the model (Sect. S1), as well as the calculation of the number concentrations of the different ice-nucleating particles available for freezing events (Sect. S2), complementing the model description in Sect. 2 of the paper. Additionally, figures complementing the evaluation of our model results presented in Sect. 3, Sect. 4, and Sect. 5 of the paper are shown here (Sect. S3). Details about each figure can be found in the corresponding sections of the paper as mentioned in the supplement figure captions.

The supplementary information presented here is in large parts based on the PhD thesis by C. G. Beer (Beer, 2021) and some of the text and the figures appeared similarly therein.

## S1 Ammonium sulfate phase transition

A schematic overview of the representation of ammonium sulfate in EMAC-MADE3 and its phase transition formulation is presented in Fig. S1. Calculations concerning ammonium sulfate are performed by the subroutines `update_amsu` and `amsu_phasetrans`, which are part of the MADE3 submodel and require input from the MESSy submodels PTRAC, MADE3, and CLOUD. A detailed description of these calculations is presented below.

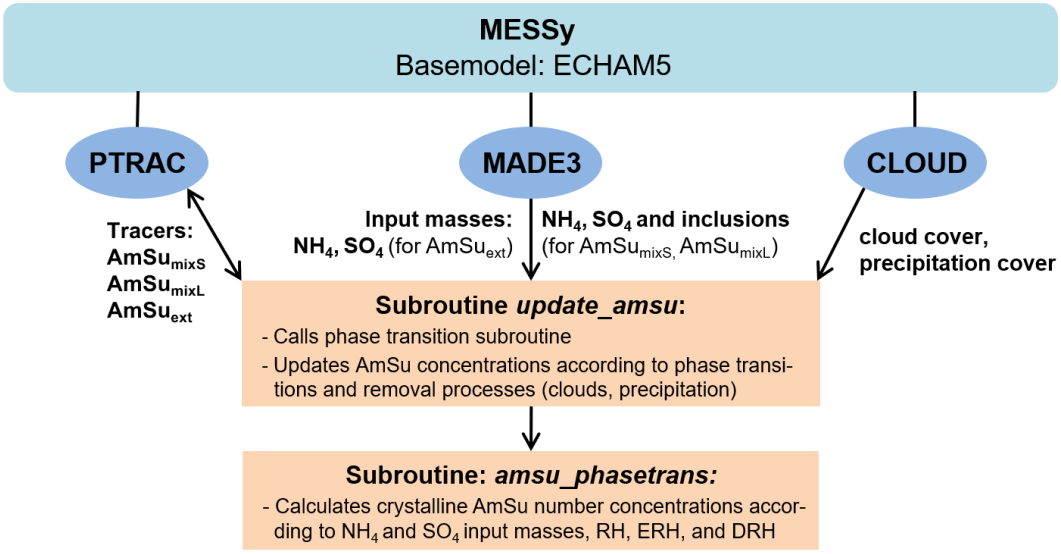


**Figure S1.** Schematic overview of the representation of AmSu tracers in EMAC-MADE3. The subroutines `update_amsu` and `amsu_phasetrans` are part of the MADE3 submodel and interact with the MESSy submodels PTRAC and CLOUD. The corresponding AmSu tracers for the coarse mode, i.e. $\mathrm{AmSu_{mix,coa}}$ and $\mathrm{AmSu_{ext,coa}}$, are not shown for the sake of simplicity.

Crystalline ammonium sulfate numbers are calculated according to $\mathrm{NH_4}$ and $\mathrm{SO_4}$ input masses from MADE3, the relative humidity, ERH and DRH. In order to exclude grid boxes with no or only little $\mathrm{NH_4}$ and $\mathrm{SO_4}$ aerosol mass contribution (for the case of $\mathrm{AmSu_{mixS}}$, $\mathrm{AmSu_{mixL}}$ tracers), only those grid boxes are taken into account, where the non-dust fraction is dominated by $\mathrm{NH_4}$ and $\mathrm{SO_4}$, i.e. where $(m_{\mathrm{NH_4}} + m_{\mathrm{SO_4}})/(m_{\mathrm{tot}} - m_{\mathrm{DU}}) \geq 0.5$. This fraction is calculated from the corresponding input masses taken from MADE3. Dust plays a special role as it facilitates crystallization (e.g. Ushijima et al., 2018). Therefore, if the non-$\mathrm{NH_4}$-$\mathrm{SO_4}$-mass is dominated by dust, i.e. $m_{\mathrm{DU}}/(m_{\mathrm{tot}} - m_{\mathrm{NH_4}} - m_{\mathrm{SO_4}}) \geq 0.5$, this effect is taken into account by an increase in ERH, as described below.

Additionally, the ammonium input mass is limited, if there is too much ammonium compared to the available sulfate, i.e. $\mathrm{NH_4}$ is scaled by $1/\mathrm{ASR}$ (for $\mathrm{ASR} > 1$), where ASR is the ammonium-to-sulfate molar ratio defined as

$$\mathrm{ASR} = \frac{[\mathrm{NH_4}]}{2\,[\mathrm{SO_4}]} \,. \tag{S1}$$

For stoichiometric reasons, this reduction represents the maximum amount of ammonium which can be transformed to the solid phase. For the case of $\mathrm{AmSu_{mixS}}$ and $\mathrm{AmSu_{mixL}}$, the mass of non-$NH_4$-$SO_4$ inclusions is calculated as

$$\mathrm{m_{incl} = m_{tot} - m_{SO_4} - m_{NH_4}} \ . \tag{S2}$$

In addition to $NH_4$, the inclusion mass has to be scaled (if $\mathrm{ASR} > 1$) by

$$\frac{m_{\mathrm{SO_4}} + m_{\mathrm{NH_4}}/\mathrm{ASR}}{m_{\mathrm{SO_4}} + m_{\mathrm{NH_4}}} \ , \tag{S3}$$

which represents the reduction of the ($SO_4$ + $NH_4$)-mass. ASR is subsequently limited to $0 \leq \mathrm{ASR} \leq 1$.

The deliquescence relative humidity is set to DRH = 80 % (Martin, 2000). Temperature dependency of DRH can be neglected, as it has only a minor influence (Onasch et al., 1999; Tang and Munkelwitz, 1993). The efflorescence relative humidity is calculated as a function of ASR according to Martin et al. (2003) and Wang et al. (2008).

$$\mathrm{ERH(ASR)} = \begin{cases} -71925 + 1690\ \mathrm{ASR} - 139\ \mathrm{ASR}^2 + \frac{1770760}{25.0 + 0.5(\mathrm{ASR} - 0.7)} \ , & \text{if } 0.5 \leq \mathrm{ASR} \leq 1.0 \\ 0 \ , & \text{if } \mathrm{ASR} < 0.5 \end{cases} \tag{S4}$$

By setting ERH to zero if $\mathrm{ASR} < 0.5$, cases where there is too much $SO_4$ for the available $NH_4$ are excluded. This implies that no crystallization is possible for $\mathrm{ASR} < 0.5$, as reported in Martin et al. (2003) and Wang et al. (2008). The temperature dependency of ERH is small and can be neglected (Onasch et al., 1999).

Equation (S4) provides a minimum ERH for the case of pure ammonium sulfate particles (without inclusions). As stated in various studies (e.g., Martin, 2000; Martin et al., 2001; Han et al., 2002; Martin et al., 2003; Pant et al., 2006; Ushijima et al., 2018), inclusions of e.g. mineral dust can increase the ERH significantly, leading to more favourable conditions for the crystalline phase. The effect of mineral dust is enhanced for larger inclusion diameters. According to Martin et al. (2003) this inclusion effect (heterogeneous nucleation) can be added to Eq. (S4) by:

$$\mathrm{ERH_{het}(ASR}, D) = \mathrm{ERH_{hom}(ASR)} + f(D) \ , \tag{S5}$$

with $f(D)$ being a function of the inclusion diameter $D$. Here, the effect of mineral dust inclusions is implemented in the following way. For $\mathrm{AmSu_{mixL}}$, ERH is increased by 10 %, if dust inclusions are present in a significant amount (dust fraction with respect to non-$SO_4$-$NH_4$ components $> 0.5$). This is in accordance with measurements from Ushijima et al. (2018) and Pant et al. (2006), where ERH is increased by approximately $10\,\%$ compared to homogeneous efflorescence for dust inclusions with diameters of about $400\ \mathrm{nm}$ (corresponding to typical MADE3 accumulation mode dust particle sizes). For simplicity, this ERH increase is assumed to be the same for $\mathrm{AmSu_{mixS}}$.

The actual ammonium sulfate phase transition is calculated in the following way. If the local RH < ERH, the total $NH_4$ and $SO_4$ mass (with possible inclusions of other components for the case of $\mathrm{AmSu_{mixS}}$ and $\mathrm{AmSu_{mixL}}$) is used to update the AmSu mass. Subsequently, this is converted to a number concentration by using the conversion function for lognormal distributions (e.g., Seinfeld and Pandis, 2016)

$$\mathrm{C}(D, \sigma_\mathrm{g}) = \frac{6}{\pi} \frac{1}{D^3 \exp(4.5 \ln^2 \sigma_\mathrm{g})\ \rho} \ , \tag{S6}$$

where $\rho$ is the component-mass-weighted mean particle density according to the mean particle density calculated in MADE3, $\sigma_g$ and $D$ are the geometric standard deviation and diameter input values specified for the AmSu tracers. In case of deliquescence, AmSu is set to zero if RH > DRH.

As AmSu tracers are removed in clouds (see the following section), the relative humidity in the cloud-free area of the grid box ($\mathrm{RH_0}$) is used for RH. $\mathrm{RH_0}$ can be calculated from the grid box mean RH ($\mathrm{RH}_m$) according to the following equations.

$$Q_m = (1 - C_\mathrm{cl})\ Q_0 + C_\mathrm{cl}\ Q_s \Rightarrow Q_0 = (Q_m - C_\mathrm{cl}\ Q_s)/(1 - C_\mathrm{cl}) \tag{S7a}$$

$$\mathrm{RH_0} = \frac{Q_0}{Q_s} = (\mathrm{RH}_m - C_\mathrm{cl})/(1 - C_\mathrm{cl}) \ , \tag{S7b}$$

with the grid box mean specific humidity $Q_m$, the cloud-free specific humidity $Q_0$, the in-cloud specific humidity $Q_s$ assumed to be equal to the saturation specific humidity, and the cloud covered fraction of the grid box $C_\mathrm{cl}$.

**Ammonium sulfate removal by clouds and precipitation**

The use of the scavenging submodel SCAV is deactivated for the AmSu tracers, since a very detailed representation of different scavenging processes is not considered necessary in this context, due to a high probability of deliquescence of crystalline ammonium sulfate in the presence of clouds and precipitation. Instead, concentration changes of AmSu tracers due to interactions with clouds and precipitation are dealt with in the following way.

AmSu is set to zero in the presence of clouds or precipitation as this implies a high probability for deliquescence due to the high relative humidity. This applies for liquid clouds, but also for the mixed phase regime where ice originates from freezing of liquid water. In the cirrus regime a different removal process is applied (as described below). Since the presence of clouds and precipitation is an indicator for enhanced relative humidity within the corresponding grid box and the simulation of clouds and precipitation is highly uncertain in global climate models, it is assumed that deliquescence occurs in the whole grid box as soon as the fraction of the grid box covered by clouds or precipitation exceeds a critical value. Here, we assume a comparatively conservative threshold value of 10 %. This conservative approach is followed (in contrast to scaling ammonium sulfate tracer changes with the cloud and precipitation free area fraction of the grid box) to avoid overestimations of crystalline ammonium sulfate numbers.

In addition to the treatment of stratiform cloud effects described above, convective clouds are dealt with by setting an additional threshold (0.1 %) for convective cloud cover ($C_{\rm cv}$, diagnostic model output estimated from the updraft strength) and corresponding removal of AmSu. The simulations are not very sensitive to this threshold, i.e. changes in AmSu concentrations of mostly a few percent when increasing the threshold for $C_{\rm cv}$ by a factor of ten. The information about cloud-covered and precipitation-covered fraction of the grid box is taken from the CLOUD submodel. A random overlap of cloud cover and precipitation cover within a grid box is assumed, i.e. the area covered by clouds or precipitation ($C_{\rm cl,pr}$) is given by:

$$C_{\rm cl,pr} = C_{\rm cl} + C_{\rm pr} - C_{\rm cl} \cdot C_{\rm pr} \ , \tag{S8}$$

with the area of the grid box covered with clouds ($C_{\rm cl}$) and precipitation ($C_{\rm pr}$), respectively.

A caveat of this procedure is that the cloud cover does not differentiate between liquid and ice clouds. For ice clouds there may possibly be no deliquescence at all. Hence, an alternative concept for handling ammonium sulfate in the cirrus regime has been implemented as described below. The same issue applies to precipitation cover. Deliquescence will happen for the case of rain, but possibly not for snow. In addition, evaporation of snow could lead to a release of AmSu. However, this process is assumed to be not very relevant for ice nucleation processes as, in many cases, those particles are released well below the cirrus level.

In cirrus clouds the relative humidity with respect to ice is potentially lower than the deliquescence humidity of ammonium sulfate, so that AmSu crystals can persist. Therefore, AmSu should be removed in the cirrus regime ($T < T_{\rm hom} = 238\,{\rm K}$) for non-deliquescence conditions only if snow formation takes place. In addition, cloud ice could possibly release crystalline ammonium sulfate after evaporation. Here, AmSu removal in cirrus clouds is implemented in the following way: The AmSu fraction that is removed by snow is calculated from the snow formation rate ($R_{\rm snow}$) and the cloud ice water content (IWC) taken from the CLOUD submodel, cloudcover ($C_{\rm cl}$), and ice active fraction of AmSu ($f_{\rm act}$):

$$f_{\rm snow} = \frac{R_{\rm snow}}{\rm IWC} \cdot C_{\rm cl} \cdot f_{\rm act} \tag{S9}$$

$f_{\rm act}$ is set to $0.01$, according to typical literature values (e.g., Ladino et al., 2014). Subsequently, AmSu concentrations are scaled with $(1 - f_{\rm snow})$. In this approach, the effect of snow impaction scavenging of AmSu particles is neglected.

## S2 Calculation of numbers of ice-nucleating aerosol particles

In Righi et al. (2020) the calculations for different freezing mechanisms in the mixed-phase and cirrus regime considering mineral dust and soot INPs are described in detail. Here, the focus is on the addition of glPOM and AmSu freezing in the cirrus regime. The existing formulation for tagged BC particles is used and adapted for BC emissions from aviation. The number of particles available for immersion freezing in mixed-phase clouds is estimated as a fraction of the number of aerosol particles activated to form cloud droplets ($N_{\mathrm{act}}$), as described in Righi et al. (2020). The number concentrations of potential INPs available for deposition nucleation and immersion freezing in cirrus clouds are indicated by $N^{\mathrm{dep(c)}}$ and $N^{\mathrm{imm(c)}}$, respectively. For AmSu and glPOM the freezing mode (deposition or immersion freezing) is uncertain and the number concentrations are defined more generally as $N^{(\mathrm{c})}$. The number concentrations of actual INPs are then calculated according to their freezing spectra depending on $S_c$ and $f_{\mathrm{act}}$ applying the Kärcher et al. (2006) parametrization.

Following the same notation as in Kaiser et al. (2019), MADE3 Aitken, accumulation, and coarse modes are indicated with the indices $k$, $a$, and $c$, respectively. Mixing states are depicted by $s$, $i$, and $m$ for soluble, insoluble, and mixed, respectively. All the calculated number concentrations undergo consistency checks in the code, to make sure that the estimated number concentrations in each mode are positive and do not exceed the total number concentration in the mode itself.

The INP properties of the mixed and insoluble Aitken modes, where no dust is present, are controlled by BC particles. The freezing efficiency of AmSu and glPOM in the Aitken modes is assumed to be low, due to the small particle size, and these INPs are neglected for the Aitken modes. In the cirrus regime, first the numbers of BCair INPs are calculated from their masses in the two different Aitken modes using the mass-to-number conversion factors from Eq. (S6) and assuming size distribution parameters typical for aircraft soot, i.e. $D = 0.025$ µm, $\sigma_g = 1.55$ for the Aitken mode and $\rho = 1500\ \mathrm{kg/m^3}$ (Petzold et al., 1999). Since no dust is present in this mode, the remaining number of particles in the mode is then assigned to BC (from non-aircraft sources).

$$N^{\mathrm{imm(c)}}_{\mathrm{BCair,k}} = M_{\mathrm{BCair,km}}\, C_{\mathrm{BCair,k}} \tag{S10a}$$

$$N^{\mathrm{dep(c)}}_{\mathrm{BCair,k}} = M_{\mathrm{BCair,ki}}\, C_{\mathrm{BCair,k}} \tag{S10b}$$

$$N^{\mathrm{imm(c)}}_{\mathrm{BC,k}} = \max(0, N_{\mathrm{km}} - N^{\mathrm{imm(c)}}_{\mathrm{BCair,k}}) \tag{S10c}$$

$$N^{\mathrm{dep(c)}}_{\mathrm{BC,k}} = \max(0, N_{\mathrm{ki}} - N^{\mathrm{dep(c)}}_{\mathrm{BCair,k}}) \tag{S10d}$$

The formulations and representations assumed for potential INPs in the accumulation modes are depicted schematically in Fig. S2. The corresponding calculations are summarized in Table S1 and Table S2 and are described in detail below.

In the soluble accumulation mode, no DU or BC are present. The number concentration of glPOM potential INPs is calculated from the glPOM mass according to Eq. (S6), assuming $D = 0.2$ µm, $\sigma_g = 2.0$ (this represents typical accumulation mode sizes and is chosen to be comparable to the assumptions for AmSu) and $\rho = 1000\ \mathrm{kg/m^3}$ (as for the MADE3 POM tracer).

$$N^{(\mathrm{c})}_{\mathrm{glPOM,as}} = M_{\mathrm{glPOM,as}}\, C_{\mathrm{glPOM,as}} \tag{S11}$$

For ammonium sulfate freezing, the number concentration of the AmSu tracers in the mode is used. The contribution of the $\mathrm{AmSu_{mixS}}$ and $\mathrm{AmSu_{mixL}}$ tracers for this mode is calculated according to the MADE3 $\mathrm{NH_4}$ and $\mathrm{SO_4}$ mass concentrations.

$$N^{\mathrm{as}}_{\mathrm{AmSu_{mix}}} = f_{\mathrm{as}} \cdot (N_{\mathrm{AmSu_{mixS}}} + N_{\mathrm{AmSu_{mixL}}}) \ , \tag{S12}$$

where $f_{\mathrm{as}}$ is the fractional contribution of the soluble accumulation mode to the total accumulation mode $\mathrm{NH_4}$ and $\mathrm{SO_4}$ mass, calculated as

$$f_{\mathrm{as}} = \frac{m^{\mathrm{as}}_{\mathrm{NH_4}} + m^{\mathrm{as}}_{\mathrm{SO_4}}}{m^{\mathrm{as}}_{\mathrm{NH_4}} + m^{\mathrm{as}}_{\mathrm{SO_4}} + m^{\mathrm{am}}_{\mathrm{NH_4}} + m^{\mathrm{am}}_{\mathrm{SO_4}}} \ . \tag{S13}$$

Subsequently, this number is reduced by the number of glPOM INPs in the mode (assuming a maximum neutralization efficiency of the AmSu INPs due to glPOM shells formed by interactions of AmSu with organic aerosols) to obtain the number of

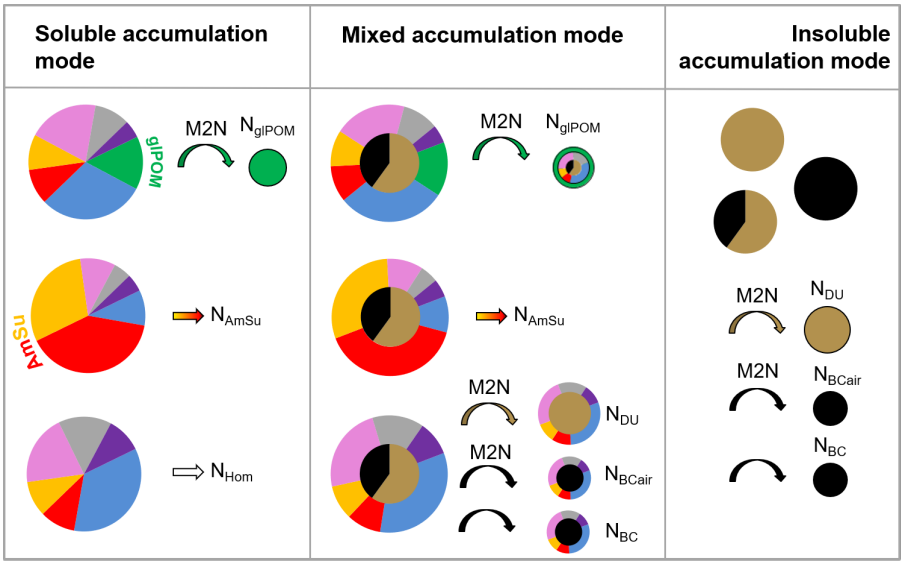


**Figure S2.** Schematic representation of assumed potential INPs concerning the calculation of number concentrations available for freezing processes in the accumulation modes. In the Aitken and coarse modes other sets of possible INP-types are participating, e.g. no AmSu and glPOM freezing in the Aitken modes, and no BCair freezing in the coarse mode is assumed. M2N represents the conversion of aerosol mass to number concentrations using Eq. (S6). Ammonium sulfate is represented in red and yellow, BC and DU in black and brown, respectively. In addition to glPOM (green), other POM may also be present but is omitted here, for the sake of simplicity. Other aerosol species simulated by MADE3 are nitrate (purple), sodium (gray), chloride (pink), and aerosol water (blue).

potential AmSu INPs in the mode.

$$N^{(c)}_{\mathrm{AmSu,as}} = \max(0, N^{\mathrm{as}}_{\mathrm{AmSu_{mix}}} - N^{(c)}_{\mathrm{glPOM,as}}) \tag{S14}$$

Additionally, the number concentration of soluble aerosols available for homogeneous freezing in the mode ($N_{\mathrm{hom,as}}$) is reduced by AmSu and glPOM numbers. For AmSu this reduction is dependent on the relation between the ice supersaturation for homogeneous freezing ($S_{\mathrm{hom}}$; Koop et al., 2000) and the deliquescence relative humidity. If $S_{\mathrm{hom}} \geq \mathrm{DRH}$ only the ice active fraction of AmSu ($f_{\mathrm{act}}$) is subtracted, as the remaining particles would be liquid and available for homogeneous freezing.

$$N_{\mathrm{hom,as}} = \begin{cases} \max(0, N_{\mathrm{as}} - N^{(c)}_{\mathrm{glPOM,as}} - N^{\mathrm{as}}_{\mathrm{AmSu_{mix}}}) \,, & \text{if } S_{\mathrm{hom}} < \mathrm{DRH} \\ \max(0, N_{\mathrm{as}} - N^{(c)}_{\mathrm{glPOM,as}} - f_{\mathrm{act}} \cdot N^{\mathrm{as}}_{\mathrm{AmSu_{mix}}}) \,, & \text{if } S_{\mathrm{hom}} \geq \mathrm{DRH} \end{cases} \tag{S15}$$

In the mixed accumulation mode all possible INPs can be present, i.e. DU, BC, AmSu, glPOM. First, the numbers of glassy organics are calculated from their mass, assuming a 50 nm thick spherical glPOM shell around a 100 nm core. This size corresponds to the assumption used for AmSu particle sizes, to keep these INP-types comparable. Following a simple geometric calculation, such a shell has an equivalent volume as a sphere with $D = 191$ nm. Together with $\sigma_g = 2.0$ and $\rho = 1000\ \mathrm{kg/m^3}$ this diameter is used to convert glPOM mass to number concentration using Eq.( S6).

$$N^{(c)}_{\mathrm{glPOM,am}} = M_{\mathrm{glPOM,am}}\, C_{\mathrm{glPOM,am}} \tag{S16}$$

The number concentration of potential AmSu INPs is again calculated as the fraction of AmSu tracers in this mode:

$$N^{(c)}_{\mathrm{AmSu,am}} = (1 - f_{\mathrm{as}}) \cdot (N_{\mathrm{AmSu_{mixS}}} + N_{\mathrm{AmSu_{mixL}}}) \tag{S17}$$

The numbers of potential BCair and DU INPs are calculated similarly, with the assumption of $D = 0.15$ µm, $\sigma_g = 1.65$ and $\rho = 1500$ kg/m$^3$ for BCair (Petzold et al., 1999) and $D = 0.42$ µm, $\sigma_g = 1.59$ and $\rho = 2500$ kg/m$^3$ for DU following the AeroCom recommendations (Dentener et al., 2006). These parameters for DU are the same that are also used to calculate the number of emitted dust particles in the model (see Beer et al., 2020, for details), i.e. the ageing of dust particles due to coagulation is neglected, which is regarded as a viable simplification due to the comparably low number concentration of dust particles in the atmosphere and the resulting low coagulation efficiency. Additionally, the numbers of DU and BCair immersion freezing INPs have to be reduced according to the respective inclusions inside AmSu particles ($N_{\mathrm{incl}}^{\mathrm{DU}}, N_{\mathrm{incl}}^{\mathrm{BCair}}$). Therefore, DU and BCair numbers are calculated as:

$$N_{\mathrm{DU,am}}^{\mathrm{imm(c)}} = \max(0, M_{\mathrm{DU,am}}\, C_{\mathrm{DU,a}} - N_{\mathrm{incl}}^{\mathrm{DU}}) \tag{S18a}$$

$$N_{\mathrm{BCair,am}}^{\mathrm{imm(c)}} = \max(0, M_{\mathrm{BCair,am}}\, C_{\mathrm{BCair,a}} - N_{\mathrm{incl}}^{\mathrm{BCair}}) \ , \tag{S18b}$$

with

$$N_{\mathrm{incl}}^{\mathrm{DU}} = \frac{N_{\mathrm{DU,am}}}{N_{\mathrm{am}}} \cdot N_{\mathrm{AmSu,am}}^{\mathrm{imm(c)}} \tag{S19a}$$

$$N_{\mathrm{incl}}^{\mathrm{BCair}} = \frac{N_{\mathrm{BCair,am}}}{N_{\mathrm{am}}} \cdot N_{\mathrm{AmSu,am}}^{\mathrm{imm(c)}} \ . \tag{S19b}$$

Subsequently, the numbers of potential DU, BCair, and AmSu INPs have to be reduced according to glPOM numbers and the assumption of glPOM forming a shell around other particles (e.g. Smith et al., 2012, 2013; Schill et al., 2014; Saukko et al., 2015). Their numbers are reduced by multiplication with the scaling factor

$$f_{\mathrm{glPOM}}^{\mathrm{am}} = (N_{\mathrm{am}} - N_{\mathrm{glPOM,am}}^{\mathrm{(c)}})/N_{\mathrm{am}} \ . \tag{S20}$$

The number of BC particles available for immersion freezing is finally calculated as the remaining number in the mode:

$$N_{\mathrm{BC,am}}^{\mathrm{imm(c)}} = \max(0, N_{\mathrm{am}} - N_{\mathrm{DU,am}}^{\mathrm{imm(c)}} - N_{\mathrm{BCair,am}}^{\mathrm{imm(c)}} - N_{\mathrm{glPOM,am}}^{\mathrm{(c)}} - N_{\mathrm{AmSu,am}}^{\mathrm{(c)}}) \tag{S21}$$

Here, BC particles are assumed to have accumulation mode sizes. Note that BC particles in the mixed accumulation mode not necessarily show accumulation mode sizes, since this mode may consist of a mixture of particles from the soluble accumulation and insoluble or mixed Aitken mode BC or BCair particles. This should be considered in the representation of the heterogeneous BC ice nucleation.

In the insoluble accumulation mode only DU, BCair and BC are present. The numbers of DU and BCair deposition freezing INPs are here again calculated from their masses, and the remaining particles in the mode are ascribed to BC deposition freezing.

$$N_{\mathrm{DU,a}}^{\mathrm{dep(c)}} = M_{\mathrm{DU,ai}}\, C_{\mathrm{DU,a}} \tag{S22a}$$

$$N_{\mathrm{BCair,a}}^{\mathrm{dep(c)}} = M_{\mathrm{BCair,ai}}\, C_{\mathrm{BCair,a}} \tag{S22b}$$

$$N_{\mathrm{BC,a}}^{\mathrm{dep(c)}} = \max(0, N_{\mathrm{ai}} - N_{\mathrm{DU,a}}^{\mathrm{dep(c)}} - N_{\mathrm{BCair,a}}^{\mathrm{dep(c)}}) \tag{S22c}$$

Calculations for the soluble coarse mode, concerning immersion freezing of glPOM and AmSu, and homogeneous freezing of solution droplets, are performed similar to those in the soluble accumulation mode, but with different assumptions for the parameters used for mass-to-number conversion of glPOM particles, i.e. $D = 2.0$ µm, $\sigma_g = 2.2$ and $\rho = 1000$ kg/m$^3$.

$$N_{\mathrm{glPOM,cs}}^{\mathrm{(c)}} = M_{\mathrm{glPOM,cs}}\, C_{\mathrm{glPOM,cs}} \tag{S23}$$

For ammonium sulfate freezing the fraction of the $\mathrm{AmSu_{mix,coa}}$ tracer in the mode is used including the reduction according to glPOM numbers in the mode (assuming a maximum neutralization efficiency of the AmSu INPs due to glPOM shells).

$$N_{\mathrm{AmSu_{mix,coa}}}^{\mathrm{cs}} = f_{\mathrm{cs}} \cdot N_{\mathrm{AmSu_{mix,coa}}} \tag{S24a}$$

$$N_{\mathrm{AmSu,cs}}^{\mathrm{(c)}} = \max(0, N_{\mathrm{AmSu_{mix,coa}}}^{\mathrm{cs}} - N_{\mathrm{glPOM,cs}}^{\mathrm{(c)}}) \ , \tag{S24b}$$

where $f_{\mathrm{cs}}$ is the fractional contribution of the soluble coarse mode to the total accumulation mode $\mathrm{NH_4}$ and $\mathrm{SO_4}$ mass, in analogy to $f_{\mathrm{as}}$ in the accumulation modes (see Eq. S13).

Additionally, the number concentration of soluble aerosols available for homogeneous freezing in the mode ($N_{\mathrm{hom,cs}}$) is reduced by AmSu and glPOM numbers depending on $S_{\mathrm{hom}}$, DRH, and the ice active fraction of AmSu ($f_{\mathrm{act}}$) as for the soluble accumulation mode.

$$N_{\mathrm{hom,cs}} = \begin{cases} \max(0, N_{\mathrm{cs}} - N^{(\mathrm{c})}_{\mathrm{glPOM,cs}} - N^{\mathrm{cs}}_{\mathrm{AmSu_{mix,coa}}}) \,, & \text{if } S_{\mathrm{hom}} < \mathrm{DRH} \\ \max(0, N_{\mathrm{cs}} - N^{(\mathrm{c})}_{\mathrm{glPOM,cs}} - f_{\mathrm{act}} \cdot N^{\mathrm{cs}}_{\mathrm{AmSu_{mix,coa}}}) \,, & \text{if } S_{\mathrm{hom}} \geq \mathrm{DRH} \end{cases} \tag{S25}$$

In the mixed coarse mode DU, BC, glPOM, and AmSu INPs may be present. In this mode it is assumed that there is no contribution of BCair particles to the number concentrations since these particles are too small to cause a mass dominance within the INP material in the coarse mode. A similar calculation as in the mixed accumulation mode is performed. Here, glPOM is assumed to form a 0.5 µm thick spherical shell around a 1 µm core, which has an equivalent volume (or mass) as a sphere with $D = 1.91$ µm, $\sigma_g = 2.2$ and $\rho = 1000\ \mathrm{kg/m^3}$. For DU, $D = 1.3$ µm, $\sigma_g = 2.0$ and $\rho = 2500\ \mathrm{kg/m^3}$ are used (Dentener et al., 2006). However, as in this mode particles can be composed of dust from both the accumulation and coarse size ranges, whose relative contribution is unknown, two cases are distinguished, in analogy to Righi et al. (2020), according to the relative abundance of mineral dust. Defining the dust number fraction as

$$f_{\mathrm{DU}} = \frac{M_{\mathrm{DU,cm}}\, C_{\mathrm{DU,c}}}{N_{\mathrm{cm}}} \ , \tag{S26}$$

it is assumed that for large $f_{\mathrm{DU}}$ the mode is dominated by mineral dust. Here, coarse dust particles are assumed to calculate the number fraction, as these particles dominate the dust mass (possible mass contributions of accumulation-mode dust are small, according to Dentener et al. (2006)). For large $f_{\mathrm{DU}}$ it can be expected that other INPs have a relatively small contribution, and all particles in the mode can be regarded as possible DU INPs. Here, $f_{\mathrm{DU}} \geq 0.7$ is assumed as a dominance threshold for DU[1]. For this case, this results in:

$$N^{\mathrm{imm(c)}}_{\mathrm{DU,c}} = N_{\mathrm{cm}} \tag{S27a}$$

$$N^{\mathrm{imm(c)}}_{\mathrm{BC,c}} = N^{\mathrm{imm(c)}}_{\mathrm{glPOM,c}} = N^{\mathrm{imm(c)}}_{\mathrm{AmSu,c}} = 0 \tag{S27b}$$

If $f_{\mathrm{DU}} < 0.7$, other INPs can play a major role and similar calculations as in the mixed accumulation mode are performed.

$$N^{\mathrm{imm(c)}}_{\mathrm{glPOM,cm}} = M_{\mathrm{glPOM,cm}}\, C_{\mathrm{glPOM,cm}} \tag{S28}$$

The number concentration of possible AmSu INPs in this mode is calculated from the fraction of the $\mathrm{AmSu_{mix,coa}}$ tracer in the mode.

$$N^{(\mathrm{c})}_{\mathrm{AmSu,cm}} = (1 - f_{\mathrm{cs}}) \cdot N_{\mathrm{AmSu_{mix,coa}}} \tag{S29}$$

Potential DU INP numbers are calculated from the DU mass in the mode and subsequently reduced by respective inclusions inside AmSu particles.

$$N^{\mathrm{imm(c)}}_{\mathrm{DU,cm}} = M_{\mathrm{DU,cm}}\, C_{\mathrm{DU,c}} - N^{\mathrm{DU}}_{\mathrm{incl}} \ , \tag{S30}$$

where

$$N^{\mathrm{DU}}_{\mathrm{incl}} = \frac{N_{\mathrm{DU,cm}}}{N_{\mathrm{cm}}} \cdot N^{(\mathrm{c})}_{\mathrm{AmSu,cm}} \ . \tag{S31}$$

This represents a minimum estimate of the number of DU particles in the mode, as also accumulation-mode dust may be present due to coagulation. Additionally the potential DU and AmSu INP number concentrations have to be reduced according

[1] Righi et al. (2020) performed a sensitivity study and showed that lower threshold values for $f_{\mathrm{DU}}$ (0.5 and 0.6) do not significantly affect the results.

to glPOM numbers following the assumption of an organic shell around other particles (e.g. Smith et al., 2012, 2013; Schill et al., 2014; Saukko et al., 2015), by multiplication with the scaling factor

$$f_{\mathrm{glPOM}}^{\mathrm{cm}} = (N_{\mathrm{cm}} - N_{\mathrm{glPOM,cm}}^{(\mathrm{c})})/N_{\mathrm{cm}} \ . \tag{S32}$$

The remaining particles in the mode are available for immersion freezing of BC, as the possible contribution of accumulation-mode dust is probably small in this non-dust-dominated regime

$$N_{\mathrm{BC,cm}}^{\mathrm{imm(c)}} = \max(0, N_{\mathrm{cm}} - N_{\mathrm{DU,cm}}^{\mathrm{imm(c)}} - N_{\mathrm{glPOM,cm}}^{\mathrm{imm(c)}} - N_{\mathrm{AmSu,cm}}^{\mathrm{imm(c)}}) \ . \tag{S33}$$

The insoluble coarse mode is dominated by mineral dust, since coagulational growth of BC particles from the insoluble accumulation mode can be neglected (limited BC mass and low self-coagulation efficiency). Therefore, the number of available deposition freezing dust INPs is given by:

$$N_{\mathrm{DU,c}}^{\mathrm{dep(c)}} = N_{\mathrm{ci}} \tag{S34}$$

**Table S1.** Overview of the calculations of INP number concentrations per MADE3 mode and INP species. MADE3 Aitken, accumulation, and coarse modes are indicated with the indices $k$, $a$, and $c$, respectively. Mixing states are depicted by $s$, $i$, and $m$ for soluble, insoluble, and mixed, respectively. All calculated number concentrations undergo consistency checks in the code, to make sure that the estimated number concentrations in each mode are positive and do not exceed the total number concentration in the mode itself. A detailed description of these calculations is presented in the text.

| Mode | | DU | BCair | glPOM | AmSu | BC |
|---|---|---|---|---|---|---|
| km | | 0 | $M_{\mathrm{BCair,km}}\, C_{\mathrm{BCair,k}}$ | 0 | 0 | $N_{\mathrm{km}} - N^{\mathrm{imm(c)}}_{\mathrm{BCair,k}}$ |
| ki | | 0 | $M_{\mathrm{BCair,ki}}\, C_{\mathrm{BCair,k}}$ | 0 | 0 | $N_{\mathrm{ki}} - N^{\mathrm{dep(c)}}_{\mathrm{BCair,k}}$ |
| ks | | 0 | 0 | 0 | 0 | 0 |
| as | | 0 | 0 | $M_{\mathrm{glPOM,as}}\, C_{\mathrm{glPOM,as}}$ | $f_{\mathrm{as}} \cdot (N_{\mathrm{AmSu_{mixS}}} + N_{\mathrm{AmSu_{mixL}}}) - N^{(\mathrm{c})}_{\mathrm{glPOM,as}}$ | 0 |
| am | | $(M_{\mathrm{DU,am}}\, C_{\mathrm{DU,a}} - N^{\mathrm{DU}}_{\mathrm{incl}}) \cdot f^{\mathrm{am}}_{\mathrm{glPOM}}$ | $(M_{\mathrm{BCair,am}}\, C_{\mathrm{BCair,a}} - N^{\mathrm{BCair}}_{\mathrm{incl}}) \cdot f^{\mathrm{am}}_{\mathrm{glPOM}}$ | $M_{\mathrm{glPOM,am}}\, C_{\mathrm{glPOM,am}}$ | $(1 - f_{\mathrm{as}}) \cdot (N_{\mathrm{AmSu_{mixS}}} + N_{\mathrm{AmSu_{mixL}}}) \cdot f^{\mathrm{am}}_{\mathrm{glPOM}}$ | $N_{\mathrm{am}} - N^{\mathrm{imm(c)}}_{\mathrm{DU,am}} - N^{\mathrm{imm(c)}}_{\mathrm{BCair,am}} - N^{(\mathrm{c})}_{\mathrm{glPOM,am}} - N^{(\mathrm{c})}_{\mathrm{AmSu,am}}$ |
| ai | | $M_{\mathrm{DU,ai}}\, C_{\mathrm{DU,a}}$ | $M_{\mathrm{BCair,ai}}\, C_{\mathrm{BCair,a}}$ | 0 | 0 | $N_{\mathrm{ai}} - N^{\mathrm{dep(c)}}_{\mathrm{DU,a}} - N^{\mathrm{dep(c)}}_{\mathrm{BCair,a}}$ |
| cs | | 0 | 0 | $M_{\mathrm{glPOM,cs}}\, C_{\mathrm{glPOM,cs}}$ | $f_{\mathrm{cs}} \cdot N_{\mathrm{AmSu_{mix,coa}}} - N^{(\mathrm{c})}_{\mathrm{glPOM,cs}}$ | 0 |
| cm | $f_{\mathrm{DU}} \geq 0.7$ | $N_{\mathrm{cm}}$ | 0 | 0 | 0 | 0 |
| | $f_{\mathrm{DU}} < 0.7$ | $(M_{\mathrm{DU,cm}}\, C_{\mathrm{DU,c}} - N^{\mathrm{DU}}_{\mathrm{incl}}) \cdot f^{\mathrm{cm}}_{\mathrm{glPOM}}$ | 0 | $M_{\mathrm{glPOM,cm}}\, C_{\mathrm{glPOM,cm}}$ | $(1 - f_{\mathrm{cs}}) \cdot N_{\mathrm{AmSu_{mix,coa}}} \cdot f^{\mathrm{cm}}_{\mathrm{glPOM}}$ | $N_{\mathrm{cm}} - N^{\mathrm{imm(c)}}_{\mathrm{DU,cm}} - N^{\mathrm{imm(c)}}_{\mathrm{glPOM,cm}} - N^{\mathrm{imm(c)}}_{\mathrm{AmSu,cm}}$ |
| ci | | $N_{\mathrm{ci}}$ | 0 | 0 | 0 | 0 |

**Table S2.** Overview of the parameters used to convert particle mass to number concentrations (using Eq. S6) per INP species and aerosol mode, i.e. particle diameter $D$, geometric standard deviation $\sigma_g$, and particle density $\rho$. MADE3 aerosol modes are abbreviated as in Table S1. For Amsu and BC particles, no mass-to-number conversion is necessary since AmSu is already a number density tracer and the BC number concentration is calculated as the remaining number in the respective mode.

| Aerosol mode | INP species | $D$ (µm) | $\sigma_g$ | $\rho$ ($\mathrm{kg/m^3}$) | Reference |
|---|---|---|---|---|---|
| km, ki | BCair | 0.025 | 1.55 | 1500 | Petzold et al. (1999) |
| as | glPOM | 0.2 | 2.0 | 1000 | $D$, $\sigma$ similar to assumptions for AmSu particles (see Sect. 3.3 of the main paper), $\rho$ according to the standard POM tracer (Kaiser et al., 2019) |
| am | glPOM | 0.191 | 2.0 | 1000 | $50\ \mathrm{nm}$ thick spherical shell around a $100\ \mathrm{nm}$ core, similar to assumed AmSu particle size (see Sect. 3.3 of the main paper) |
| | BCair | 0.15 | 1.65 | 1500 | Petzold et al. (1999) |
| | DU | 0.42 | 1.59 | 2500 | Dentener et al. (2006) |
| ai | BCair | 0.15 | 1.65 | 1500 | Petzold et al. (1999) |
| | DU | 0.42 | 1.59 | 2500 | Dentener et al. (2006) |
| cs | glPOM | 2.0 | 2.2 | 1000 | $D$, $\sigma$ similar to assumptions for AmSu particles (see Sect. 3.3 of the main paper), $\rho$ according to the standard POM tracer (Kaiser et al., 2019) |
| cm | glPOM | 1.91 | 2.2 | 1000 | $0.5\ \mathrm{µm}$ thick spherical shell around a $1\ \mathrm{µm}$ core, similar to assumed AmSu particle size (see Sect. 3.3 of the main paper) |
| | DU | 1.3 | 2.0 | 2500 | Dentener et al. (2006) |

## S3 Supplementary figures

The following figures complement the evaluation of the results presented in Sect. 3, Sect. 4, and Sect. 5 of the paper.

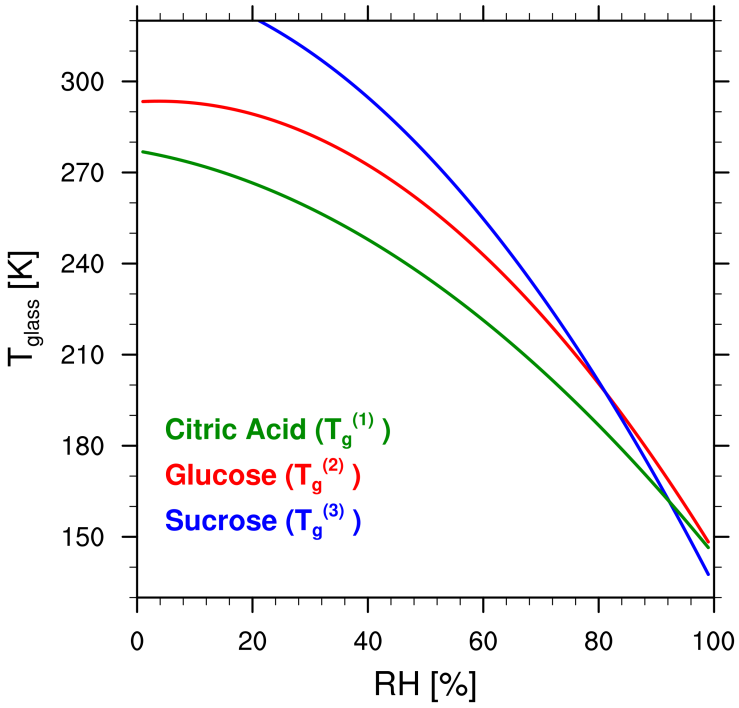


**Figure S3.** Experimentally determined $T_g(\mathrm{RH})$ curves according to Baustian et al. (2013) for the three different SOA proxies used in this study, i.e. citric acid (green), glucose (red), and sucrose (blue). See Sect. 3.2 in the paper for details.

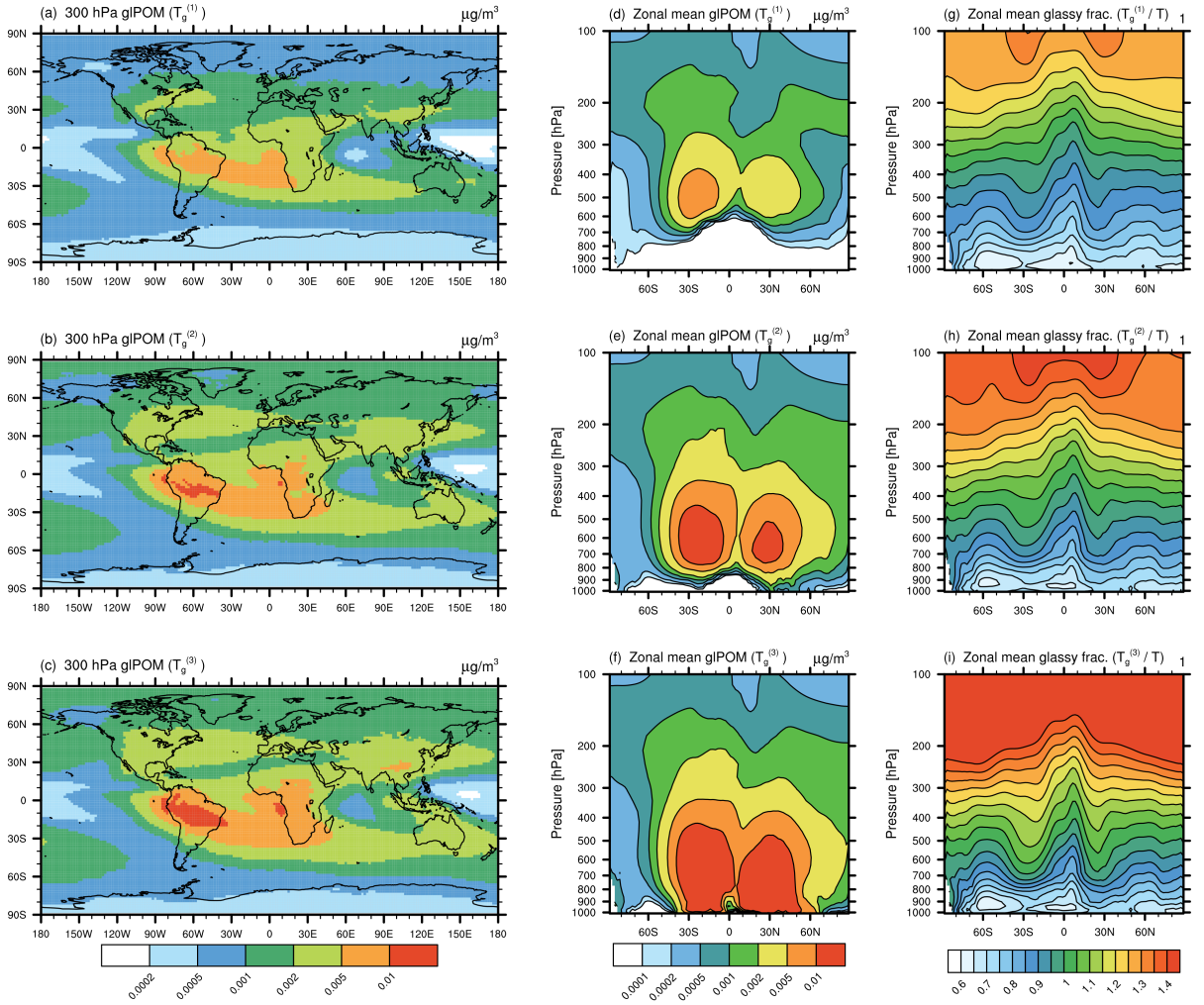


**Figure S4.** Similar to Fig. 2 but showing the global distribution of glPOM at the 300 hPa level in units of $\mu g\,m^{-3}$ (a, b, c), the zonally averaged vertical distribution of the glass transition temperature $T_g$ in units of K (d, e, f), and the corresponding ratio $T_g/T$ (g, h, i) for the three different representations of $T_g(\mathrm{RH})$. See Sect. 3.2 in the paper for details.

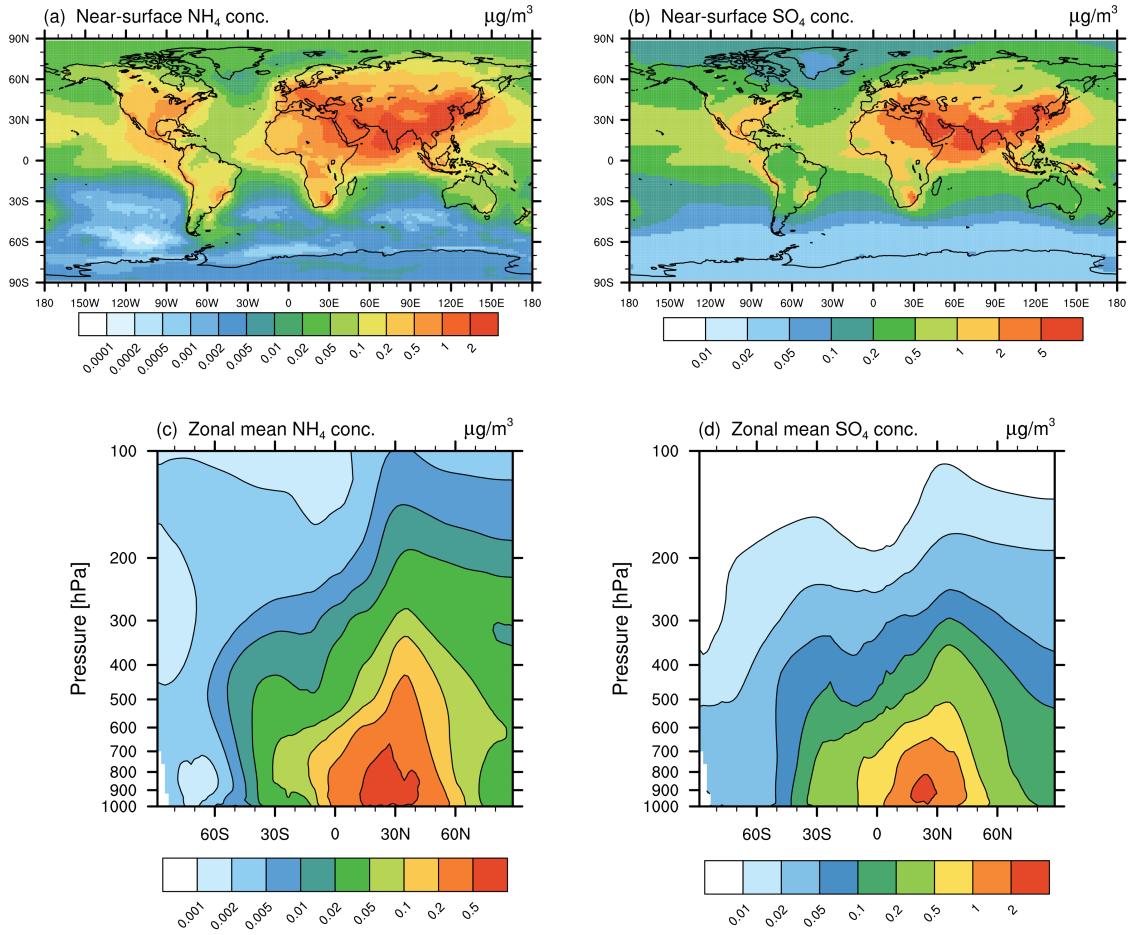


**Figure S5.** Global distribution of simulated mass concentrations of ammonium ($NH_4$) and sulfate ($SO_4$) (multi-annual mean, years 2010–2019). Mass concentrations in units of $\mu g\,m^{-3}$ are shown near the surface (a, b) and as zonal mean vertical distribution (c, d) for $NH_4$ and $SO_4$, respectively. See Sect. 4.3 in the paper for details.

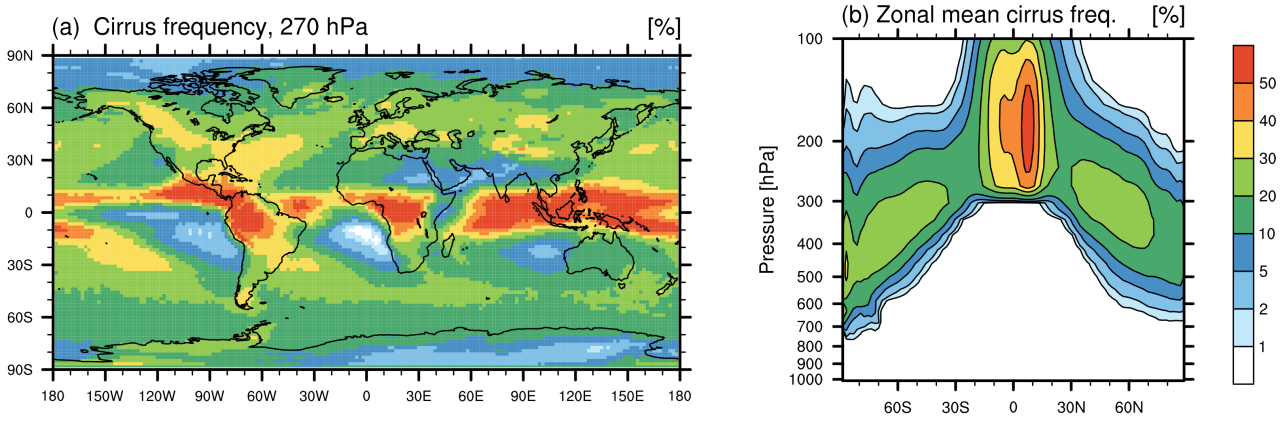


**Figure S6.** Global distribution of simulated cirrus cloud occurrence frequency (multi-annual mean, years 2010–2019) calculated according to temperature ($T < -35\ ^{\circ}\mathrm{C}$) and ice water content (IWC $> 0.5\ \mathrm{mg\,kg^{-1}}$), showing (a) cirrus frequency at 270 $\mathrm{hPa}$ and (b) zonal-mean cirrus frequency. See Sect. 5 in the paper for details.

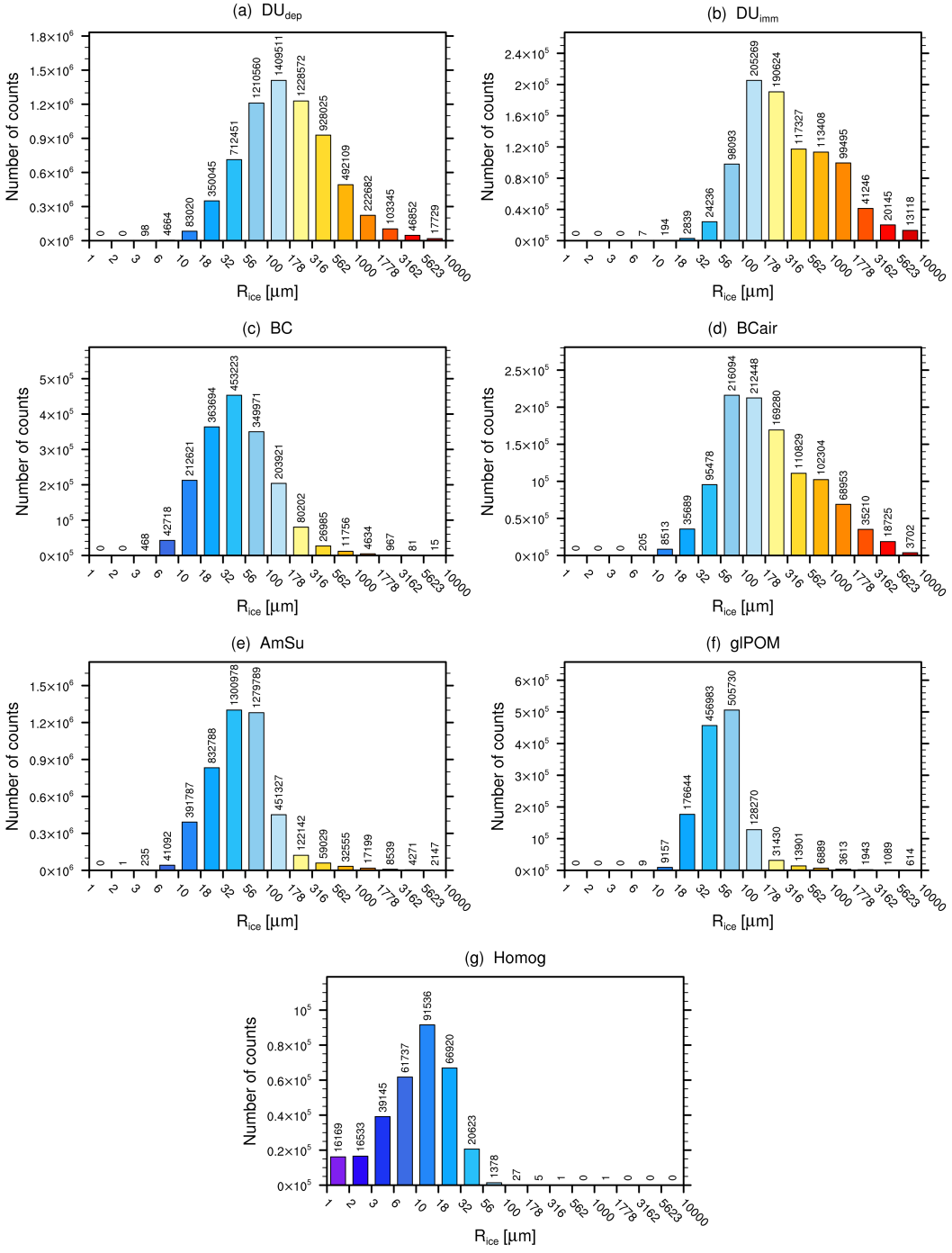


**Figure S7.** Simulated ice crystal radii (in units of µm) of newly formed crystals per freezing mode. The histograms are calculated from one simulated year (using the original 11-hourly model output), with four logarithmic bins per order of magnitude. Shown are (a) DU immersion, (b) DU deposition, (c) BC, (d) BCair, (e) AmSu, (f) glPOM, and (g) homogeneous freezing. Numbers above each bar represent actual counts. Note the different y-axis scales in each plot. See Sect. 5 in the paper for details.

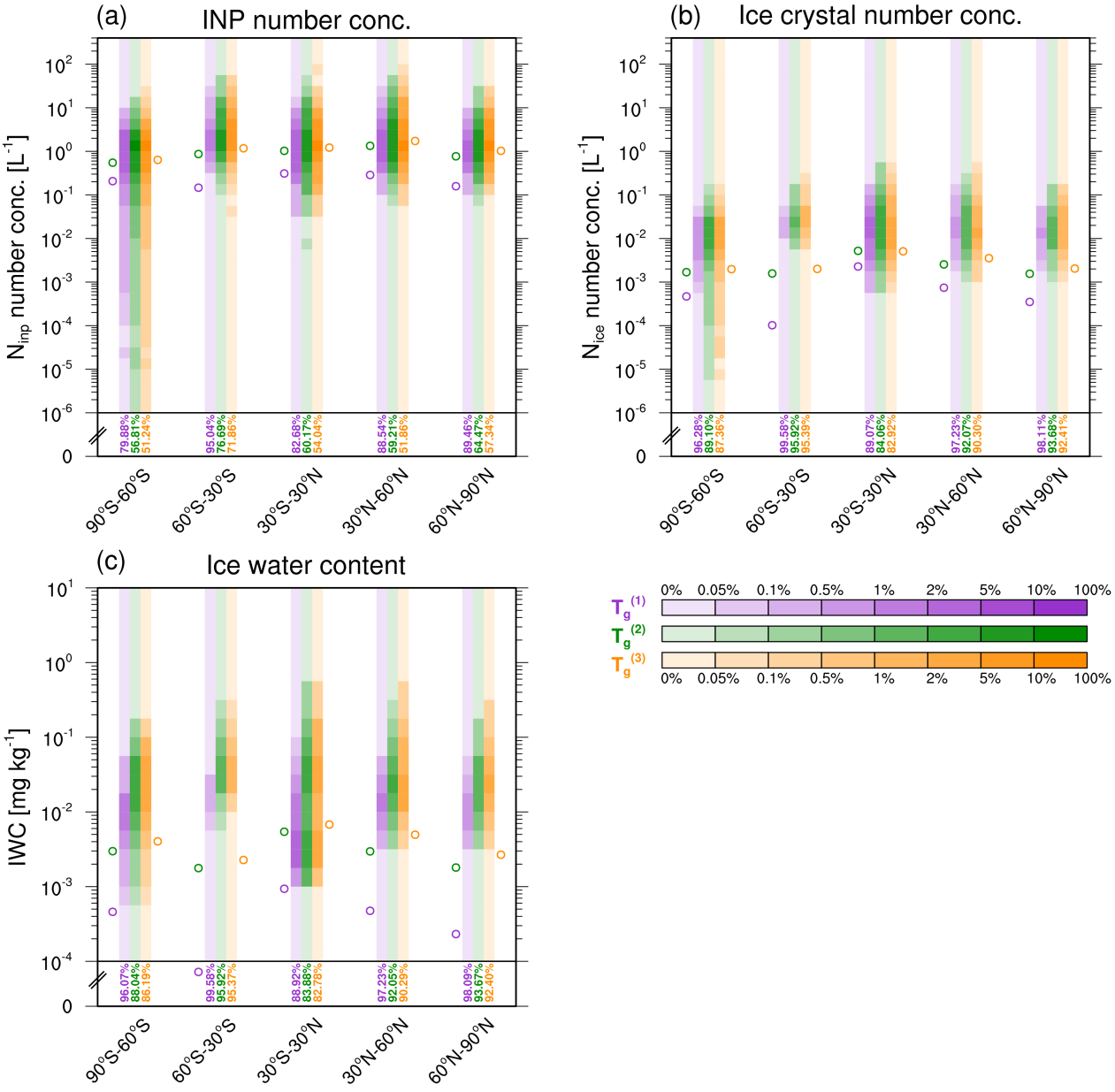


**Figure S8.** Similar to Fig. 6, but showing INP number concentrations, number concentrations and ice water content of pristine ice crystals for the three different representations of $T_g(\mathrm{RH})$ for glPOM, considering the SOA proxies citric acid ($T_g^{(1)}$), glucose ($T_g^{(2)}$), and sucrose ($T_g^{(3)}$). See Sect. 5 in the paper for details.

## References


Beer, C. G.: Global modelling of ice nucleating particles and their effects on cirrus clouds, Ph.D. thesis, Ludwig-Maximilians-Universität München, https://doi.org/10.5282/edoc.28470, 2021.

Beer, C. G., Hendricks, J., Righi, M., Heinold, B., Tegen, I., Groß, S., Sauer, D., Walser, A., and Weinzierl, B.: Modelling mineral dust emissions and atmospheric dispersion with MADE3 in EMAC v2.54, Geosci. Model Dev., 13, 4287–4303, https://doi.org/10.5194/gmd-13-4287-2020, 2020.

Dentener, F., Kinne, S., Bond, T., Boucher, O., Cofala, J., Generoso, S., Ginoux, P., Gong, S., Hoelzemann, J., Ito, A., et al.: Emissions of primary aerosol and precursor gases in the years 2000 and 1750 prescribed data-sets for AeroCom, Atmos. Chem. Phys., 6, 4321–4344, https://doi.org/10.5194/acp-6-4321-2006, 2006.

Han, J.-H., Hung, H.-M., and Martin, S. T.: Size effect of hematite and corundum inclusions on the efflorescence relative humidities of aqueous ammonium nitrate particles, J. Geophys. Res., 107, AAC 3–1–AAC 3–9, https://doi.org/10.1029/2001JD001054, 2002.

Kaiser, J. C., Hendricks, J., Righi, M., Jöckel, P., Tost, H., Kandler, K., Weinzierl, B., Sauer, D., Heimerl, K., Schwarz, J. P., Perring, A. E., and Popp, T.: Global aerosol modeling with MADE3 (v3.0) in EMAC (based on v2.53): model description and evaluation, Geosci. Model Dev., 12, 541–579, https://doi.org/10.5194/gmd-12-541-2019, 2019.

Kärcher, B., Hendricks, J., and Lohmann, U.: Physically based parameterization of cirrus cloud formation for use in global atmospheric models, J. Geophys. Res. Atmos., 111, D01 205, https://doi.org/10.1029/2005JD006219, 2006.

Koop, T., Luo, B., Tsias, A., and Peter, T.: Water activity as the determinant for homogeneous ice nucleation in aqueous solutions, Nature, 406, 611, https://doi.org/10.1038/35020537, 2000.

Ladino, L. A., Zhou, S., Yakobi-Hancock, J. D., Aljawhary, D., and Abbatt, J. P. D.: Factors controlling the ice nucleating abilities of $\alpha$-pinene SOA particles, J. Geophys. Res. Atmos., 119, 9041–9051, https://doi.org/10.1002/2014JD021578, 2014.

Martin, S. T.: Phase Transitions of Aqueous Atmospheric Particles, Chem. Rev., 100, 3403–3454, https://doi.org/10.1021/cr990034t, 2000.

Martin, S. T., Han, J.-H., and Hung, H.-M.: The size effect of hematite and corundum inclusions on the efflorescence relative humidities of aqueous ammonium sulfate particles, Geophys. Res. Lett., 28, 2601–2604, https://doi.org/10.1029/2001GL013120, 2001.

Martin, S. T., Schlenker, J. C., Malinowski, A., Hung, H.-M., and Rudich, Y.: Crystallization of atmospheric sulfate-nitrate-ammonium particles, Geophys. Res. Lett., 30, 1–6, https://doi.org/10.1029/2003GL017930, 2003.

Onasch, T. B., Siefert, R. L., Brooks, S. D., Prenni, A. J., Murray, B., Wilson, M. A., and Tolbert, M. A.: Infrared spectroscopic study of the deliquescence and efflorescence of ammonium sulfate aerosol as a function of temperature, J. Geophys. Res., 104, 21 317–21 326, https://doi.org/10.1029/1999JD900384, 1999.

Pant, A., Parsons, M. T., and Bertram, A. K.: Crystallization of Aqueous Ammonium Sulfate Particles Internally Mixed with Soot and Kaolinite: Crystallization Relative Humidities and Nucleation Rates, J. Phys. Chem. A, 110, 8701–8709, https://doi.org/10.1021/jp060985s, 2006.

Petzold, A., Döpelheuer, A., Brock, C. A., and Schröder, F.: In situ observations and model calculations of black carbon emission by aircraft at cruise altitude, J. Geophys. Res. Atmos., 104, 22 171–22 181, https://doi.org/10.1029/1999jd900460, 1999.

Righi, M., Hendricks, J., Lohmann, U., Beer, C. G., Hahn, V., Heinold, B., Heller, R., Krämer, M., Ponater, M., Rolf, C., Tegen, I., and Voigt, C.: Coupling aerosols to (cirrus) clouds in the global EMAC-MADE3 aerosol-climate model, Geosci. Model Dev., 13, 1635–1661, https://doi.org/10.5194/gmd-13-1635-2020, 2020.

Saukko, E., Zorn, S., Kuwata, M., Keskinen, J., and Virtanen, A.: Phase State and Deliquescence Hysteresis of Ammonium-Sulfate-Seeded Secondary Organic Aerosol, Aerosol Sci. Technol., 49, 531–537, https://doi.org/10.1080/02786826.2015.1050085, 2015.

Schill, G. P., De Haan, D. O., and Tolbert, M. A.: Heterogeneous ice nucleation on simulated secondary organic aerosol, Environ. Sci. Technol., 48, 1675–1682, https://doi.org/10.1021/es4046428, 2014.

Seinfeld, J. H. and Pandis, S. N.: Atmospheric chemistry and physics: From air pollution to climate change, John Wiley & Sons, 2016.

Smith, M. L., Bertram, A. K., and Martin, S. T.: Deliquescence, efflorescence, and phase miscibility of mixed particles of ammonium sulfate and isoprene-derived secondary organic material, Atmos. Chem. Phys., 12, 9613–9628, https://doi.org/10.5194/acp-12-9613-2012, 2012.

Smith, M. L., You, Y., Kuwata, M., Bertram, A. K., and Martin, S. T.: Phase Transitions and Phase Miscibility of Mixed Particles of Ammonium Sulfate, Toluene-Derived Secondary Organic Material, and Water, J. Phys. Chem. A, 117, 8895–8906, https://doi.org/10.1021/jp405095e, 2013.

Tang, I. N. and Munkelwitz, H. R.: Composition and temperature dependence of the deliquescence properties of hygroscopic aerosols, Atmos. Environ. Part A. General Topics, 27, 467 – 473, https://doi.org/10.1016/0960-1686(93)90204-C, 1993.

Ushijima, S. B., Davis, R. D., and Tolbert, M. A.: Immersion and Contact Efflorescence Induced by Mineral Dust Particles, J. Phys. Chem. A, 122, 1303–1311, https://doi.org/10.1021/acs.jpca.7b12075, 2018.

Wang, J., Hoffmann, A. A., Park, R. J., Jacob, D. J., and Martin, S. T.: Global distribution of solid and aqueous sulfate aerosols: Effect of the hysteresis of particle phase transitions, J. Geophys. Res. Atmos., 113, D11 206, https://doi.org/10.1029/2007JD009367, 2008.